ADVANCED OPTICAL MATERIALS
www.advopticalmat.de

All-Dielectric Insulated 3D Plasmonic Nanoparticles for Enhanced Self-Floating Solar Evaporation under One Sun

*Yang Wang, Haiyang Ma, Jianyu Yu, Jinlei Li, Ning Xu, Jia Zhu, and Lin Zhou**

Plasmonic absorbers, featured by unique capability of broadband light absorption and nanoscale optical concentration, have long been regarded as ideal candidates for self-floating interfacial solar evaporation yet suffering from low energy transfer efficiency because of poor thermal localization. In this work, by implanting an ion beam exfoliation of the continuous metallic film from the gold/nanoporous alumina template (Au/NPT), the all-dielectric insulated plasmonic absorbers are demonstrated as efficient self-floating interfacial solar evaporators with measured efficiency of ≈80% under one sun, which shows a ≈20% increment to conventional Au/NPT and is comparable to mainstream complicated carbon-based evaporators with external thermal insulators. The enhanced energy transfer process can be ascribed to synergistic effect of plasmon-enhanced solar absorption, broadband light induced thermal localization and/or insulation, as well as efficient mass transport channels. The results here would provide a new insight in underlying understanding and inspire further development of plasmonic solar thermal conversion.

1. Introduction

Plasmonic absorbers have generated tremendous excitements in the field of nanophotonics,[1] photochemistry,[2] biophotonics,[3] etc. Due to the unique capability of spectral manipulation and subwavelength light concentration,[4] plasmon-enhanced solar steam generation has inspired the revival of solar thermal conversion,[5,6] beneficial for applications ranging from solar evaporation,[7–10] sterilization,[11,12] to solar water treatment.[13–19] Versatile metallic absorbers have been devoted to approach the interfacial steam generation and thus to improve the solar thermal conversion efficiency, such as gold nanoparticle nanofluid,[6,20] gold nanowires,[21] paper or wood loaded metal particles,[22,23] and TiN nanocavities.[24] Among versatile endeavors, the 3D plasmonic absorbers consisting of nanoporous-templates (NPT)-initiated self-assembled nanoparticles have aroused most attention for its intriguing fundamental mechanism of broadband light absorption, scalable and cost-effective fabrication process of physical vapor deposition (PVD),[13,25] and multiplexed photonic functionalities.[26–29] However, lack of efficient thermal insulation and considerable heat loss from metals makes the plasmonic absorber a rather high thermal conduction loss. Such self-floating plasmonic solar evaporators (with large-area metal films directly contacted with bulk water, see **Figure 1**a) can enable merely ≈60% solar thermal efficiency under one sun illumination, far more below those of conventional carbon-based materials equipped with external thermal insulators/floaters (≳80%).[30–33] It is rather challenging but of great importance for a self-floating plasmonic solar evaporator to simultaneously enable broadband light absorption and effective thermal insulation, which is ideal for point-of-use solar thermal conversion under natural condition of solar irradiance. In this work, by ion beam exfoliating of the continuous gold (Au) film from the surface of the PVD prepared Au/NPT (noted as i-Au/NPT), we experimentally demonstrate the all dielectric embedded plasmonic nanoparticles as high-performing plasmonic solar evaporators, which enables efficient broadband light harvesting and self-heat-insulation in the same self-floating configuration without optical concentration or external thermal spacings. Because of the synergistic optical and thermal manipulation combined with improved water transportation, the measured solar thermal efficiency of the prepared solar absorber reaches ≈80% (comparable to the conventional external-floater-loaded carbonized counterparts). Particularly, the i-Au/NPT evaporator with a thickness of only tens of microns has reached an efficiency level of those carbon-based evaporators or commercial devices with thickness of several centimeters/decimeters. The proposed thermal-insulator-free high-performance solar evaporators would provide powerful strategy to scalable and cost-effective solar water purification and wastewater treatment especially for emergent application situations such as drinkable water sources for

Y. Wang, H. Ma, J. Yu, J. Li, N. Xu, J. Zhu, L. Zhou
National Laboratory of Solid State Microstructures
College of Engineering and Applied Sciences
School of Physics
Key Laboratory of Intelligent Optical Sensing and Integration
and Collaborative Innovation Center of Advanced Microstructures
Nanjing University
Nanjing 210093, P. R. China
E-mail: linzhou@nju.edu.cn
Y. Wang
Key Lab of Advanced Optoelectronic Quantum Architecture
and Measurement (Ministry of Education)
Beijing Key Lab of Nanophotonics & Ultrafine Optoelectronic Systems
and School of Physics
Beijing Institute of Technology
Beijing 100081, P. R. China
The ORCID identification number(s) for the author(s) of this article can be found under https://doi.org/10.1002/adom.202201907.

DOI: 10.1002/adom.202201907

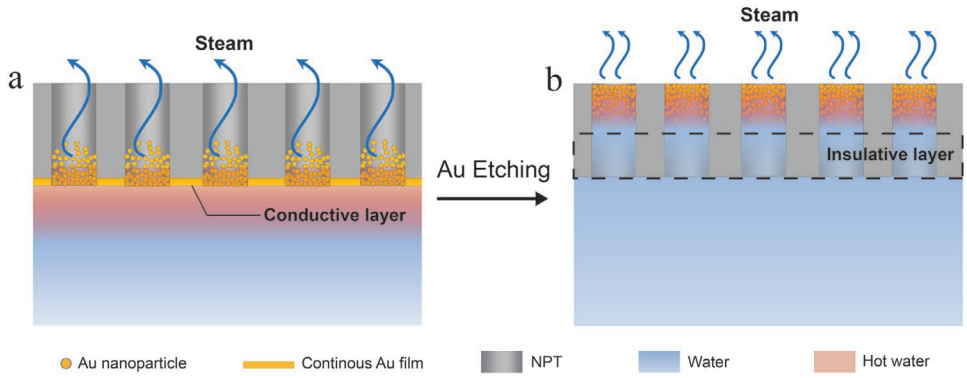

Figure 1. Schematic of the Au/NPT and i-Au/NPT as interfacial solar thermal evaporators, respectively. a) The Au/NPT. Before etching, the continuous Au side must be downward to avoid reflection loss, which makes the solar steam generation layer directly in contact with water and resulting in a large amount of heat conduction loss to bulk water due to the high thermal conductivity of continuous Au film. b) The i-Au/NPT. After etching and inverting the device, the steam generation layer is spatially decoupled with bulk water by porous alumina layer, which has a much lower thermal conductivity compared with Au film. The removal of Au film combined with inversed structure also improved the absorption of solar energy and mass transport of water.

off-grid or remote area. Our results would provide new insight to plasmon-enhanced solar thermal applications.

2. Results and Discussion

The schematic of the i-Au/NPT as an interfacial solar evaporator is demonstrated in Figure 1b, where the Au-NPT-based counterpart (noted as Au/NPT) is shown in Figure 1a as well for comparison. In order to achieve high performance of the evaporator, three crucial designs and/or treatments are needed. 1) The operation configuration should be inversed so that it is the porous dielectric layer (instead of Au particles and Au film) that is thermally conducting with bulk water. 2) The continuous Au film should be carefully removed (without destroy the inside nanoparticles) so that broadband anti-reflection of light can be enabled and more solar energy can be transferred to heat. 3) The depositing depth of Au nanoparticles inside the nanopores should be distinctly shorter than NPT thickness, ensuring a sufficient thermal spacing layer.

Based on the above structure transformations, the i-Au/NPT absorbers exhibit three benefits as self-floating plasmonic interfacial solar evaporators. 1) Reduced thermal conduction loss to bulk water. After removing the continuous Au film, the close-packed nanoparticles are completed encapsulated inside the dielectric NPT, making it thermally isolated from bulk water. The porous alumina is naturally serving as a spacing layer between the light absorbing layer and bulk water, thermally insulating the harvested solar energy from dissipating into the bulk water. 2) Efficient and broadband solar absorption. The Au nanoparticles play the most crucial role in broadband absorption in the Au/NPT plasmonic absorbers.[14] The inversed configuration makes the nanoparticles closer to the incident light, ensuring efficient and broadband solar energy absorption. In addition, the removal of Au film and large-sized nanoparticles on the surface can essentially reduce the emissivity in the mid-infrared wavelengths and thus improve the energy conversion efficiency. 3) Enhanced mass transport. The removal of Au film makes the structure more hydrophilic. Meanwhile, the evaporation spots of i-Au/NPT are located on top of the absorber surface, so that the generated solar steam can directly escape to the ambient without long-distance transporting inside the confined nanochannels. Thus, more efficient mass transport is achieved.

To verify the above design, we prepared the plasmonic absorber on the following procedures. As is shown in **Figure 2**a–c, we first assembled a large number of gold nanoparticles in NPT. Nanoporous alumina template can be prepared in a large area by standard anodizing process. Then the sample is transferred into a high vacuum PVD system for Au deposition. With appropriate deposition conditions, continuous Au film forms on the depositing surface of NPT and vertically close-packed Au nanoparticles on the side wall of the pores. The samples were then transferred into the ion beam etching (IBE) system to remove the surface Au film, and finally get our ultra-thin and self-floating plasmonic solar evaporators with enhanced photothermal regulation. We characterized the microstructure of the surface and cross-section of the samples before (Figure 2d,e) and after (Figure 2g,h) IBE treatment by scanning electron microscopy. We can see the Au film and large-size Au particles on the surface of NPT before treatment, which reflects light and makes it exhibit metallic luster in the optical image. While, the surface of the treated sample has no Au reserved, and close-packed Au nanoparticles remains on the side wall of the pore near the surface, ensuring high and broadband absorption of solar energy. The hydrophobicity of the metal hinders the transport of water to the evaporation hotspot, reducing the efficiency of the Au/NPT without IBE treatment (Figure 1a). Apart from the all-dielectric insulated 3D microstructure, we also performed the surface wettability experiment of the plasmonic evaporators before and after IBE treatment, respectively (Figure 2f,i). One may find that, the contact angle of water on the i-Au/NPT reduced to 45.8° (Figure 2i) after the continuous Au film is removed, while the contact angle of which reached 108.3° (Figure 2f) before. This ensures that water can be more fluently transported to the evaporation sites, indicating that the available evaporation area is spatially decoupled with the bulk water.

Apart from the efficient mass transport, we further demonstrate that the i-Au/NPT is ideal for interfacial solar evaporation

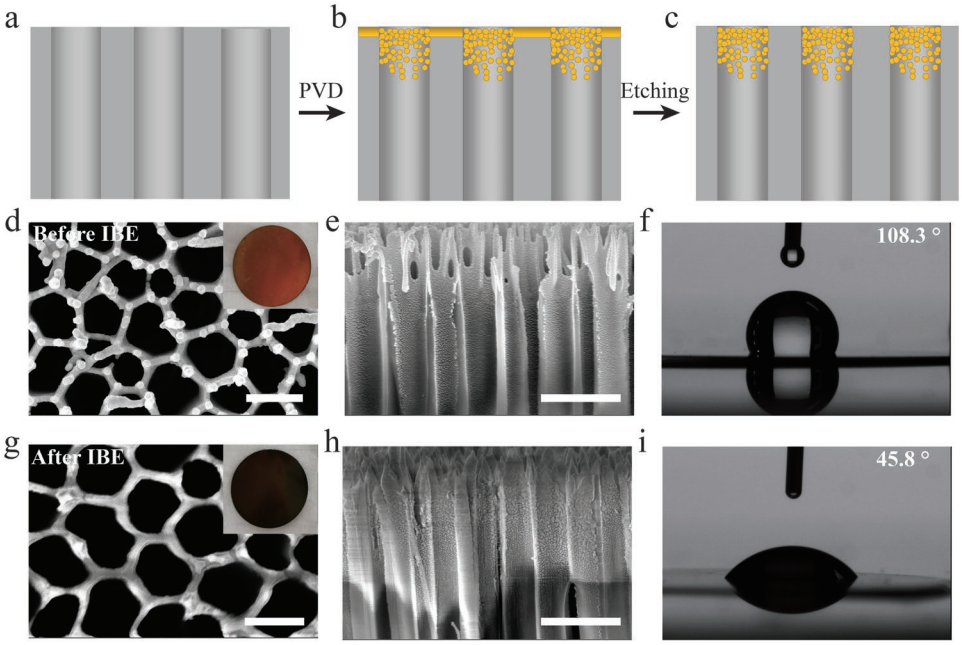

Figure 2. Microstructure characterization of IBE-treated Au/NPT (before and after). a–c) The Au/NPT structure formed after the PVD and etching. d,g) Top view SEM, scale bar: 500 and 400 nm, respectively. e,h) Cross-sectional SEM, scale bar: 1 µm. f,i) Surface wettability.

from viewpoints of optical managements. The distribution of gold film and nanoparticle on the surface of AAO is the main factor affecting the performance of spectrum and solar evaporation. We have prepared and characterized i-Au/NPT devices with different Au thickness and etching time, and found that there are mainly three different morphologies. The first is the un-etched device with continuous Au film and dispersed nanoparticles (noted as i-Au/NPT-ue); the second is partially etched device with discontinuous Au film and small number of nanoparticles (noted as i-Au/NPT-pe); the third is completely etched device with no Au film and nanoparticles (noted as i-Au/NPT-ce). As the broadband and high solar energy absorption is a prerequisite for efficient solar thermal conversion, we first measured the visible and infrared absorption spectra of all i-Au/NPT as well as Au/NPT devices with different IBE treatment (**Figure 3**a,b). It can be found that before the IBE treatment, the metal deposition side (i-Au/NPT-ue) has a lower absorption in the visible wavelengths due to surface reflection, and the reverse side (Au/NPT) has a nearly full absorption across solar spectrum as the light is absorbed by the close-packed nanoparticles before reaching the reflective layer. After partially etching, however, the solar and infrared absorptance of the i-Au/NPT-pe has reached a high level that is comparable to Au/NPT. With the increase of etching degree from partially etched to completely etched, the infrared absorptance/emittance is reduced, which is beneficial to the reduction of radiation loss of the device.

In order to explore the influence of spectral absorptance and emittance on evaporation efficiency, we calculated the power of solar energy absorption (P_{abs}), spontaneous emission (P_{rad}), and environmental energy absorption (P_{env}) of the evaporators in an atmospheric environment (Figure 3c, calculation details see Supporting Information). The removal of the continuous Au film brings different effects in different wavelengths. 1) In the visible to near-infrared band, the absorptance of etched i-Au/NPT devices remains very high compared with Au/NPT, indicating that the main structure of closed-packed Au nanoparticles has not been damaged. And a P_{abs} increment from 711 W m^{-2} (i-Au/NPT-ue) to above 951 W m^{-2} (i-Au/NPT-pe and ce) is observed. 2) The IBE treatment not only removed the continuous Au film, but also reduced the number of large-sized nanoparticles, resulting in a slight decrease in absorptance at 1.5–3 µm as the etching time increases (i-Au/NPT-pe and ce). But there is little impact on P_{abs} as the energy density of solar spectrum is very small in these wavelengths (solar irradiance shows in Figure 3a, orange area). So that a comparable value to that of Au/NPT is achieved, reaching nearly full absorption of solar energy (≈1 kW m^{-2}, Figure 3c, black square line). Compared with partially etched device, although the completely etched device has lower solar spectral absorptance due to higher etching degree, the influence of energy input is very small. 3) The mid-infrared band is the region of spontaneous emission (Figure 3b, purple area) and environment radiation. Thanks to the reduced emittance, the P_{rad} loss of i-Au/NPT-ce decreased from 366 to 351 W m^{-2}, compared with Au/NPT. While, the P_{rad} of i-Au/NPT-pe is 369 W m^{-2}, still a high value because of large-sized nanoparticles and discontinuous Au film. Meanwhile, the removal of the continuous Au film of i-Au/NPT-pe/ce exposes the alumina in the reversed structure, which enables an intrinsic absorption increase from 21 W m^{-2} to above 139 W m^{-2} from environment radiation, compared with i-Au/NPT-ue.

In a word, the etched i-Au/NPT combines the advantages of both sides of Au/NPT in spectral performance. The absorption of external energy is kept at a high level and the spontaneous emission loss is suppressed. Therefore, the final total spectral input energy ($P_{in} = P_{abs} - P_{rad} + P_{env}$) is increased with

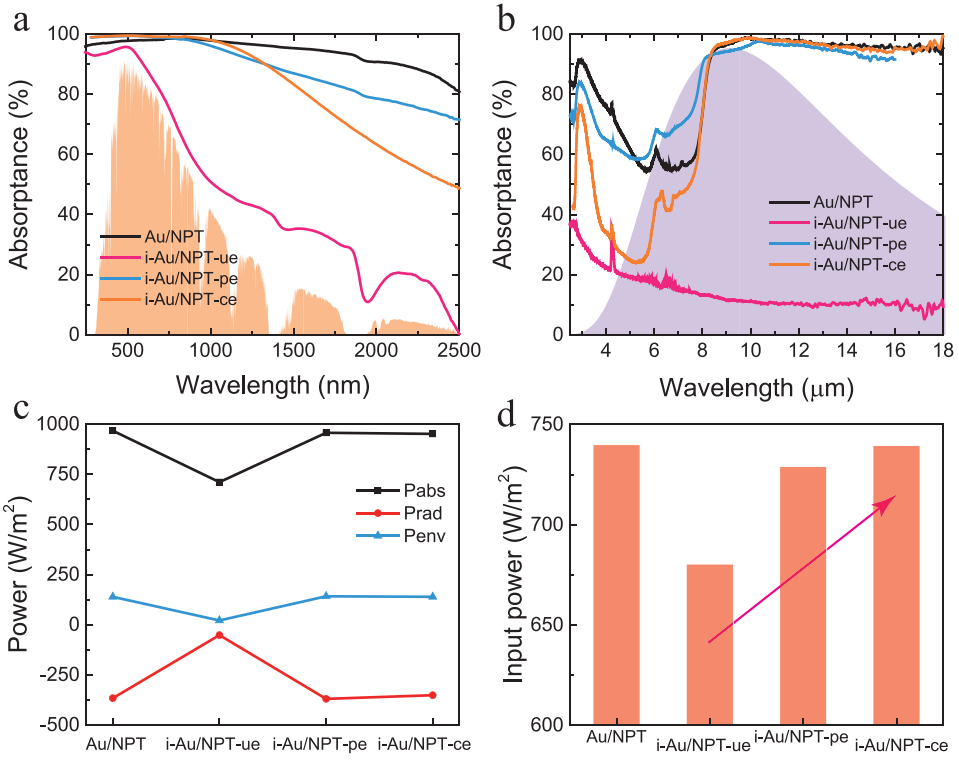

Figure 3. Optical characterization of Au/NPT before and after IBE treatment. The two sides of untreated samples are noted as Au/NPT and i-Au/NPT-ue. The partially/completely etched samples noted as Au/NPT-pe/ce, respectively. a,b) Solar absorption and thermal emission spectra of Au-NPT-based evaporators. Background shows the spectrum distribution of solar (orange) and blackbody radiation (purple). c) Power of solar absorption, radiation loss, and environmental-radiation absorption of Au-NPT-based evaporators in atmospheric environment. d) Total spectral input power of Au-NPT-based evaporators.

increase in etching degree, reaching 59 W m^{-2} increment from un-etched to completely etched (Figure 3d). This improvement makes the P_{in} of i-Au/NPT-ce comparable to Au/NPT, which ensures a high spectral energy input level in a better thermal insulated structure. Especially, when the working temperature of the evaporator is very high, the inhibition of spontaneous emission will be more obvious, which is conducive to the improvement of solar thermal efficiency.

Compared with the untreated absorber, the IBE-treated plasmonic absorber not only has improved performance in terms of mass transport and absorption spectroscopy, but also greatly improved in terms of interfacial thermal management. **Figure 4**a records the mass change of the devices for water evaporation as a function of time under one sun. The experiments show that etched i-Au/NPT's evaporation rate is significantly higher than the un-etched ones (Figure 4b). Based on the steady state evaporation rate, the solar thermal conversion efficiency can be calculated.[7,34] The efficiency of the i-Au/NPT-pe and ce reaches 79.4% and 80.5%, while the efficiency of the other two evaporators are only 71% and 51.3%, respectively. We believe that this improvement is mainly due to the optimized interfacial thermal management effect. Before IBE treatment, there is a large amount of heat conduction loss from the evaporator to water due to the high thermal conductivity of continuous Au film. Our design takes advantage of the dielectric NPT itself to achieve thermal insulation by removing the continuous Au film and inverting the device. After the Au nanoparticles are placed upward, the heat conduction loss is reduced in both horizontal and vertical directions: 1) the sidewall of NPT hinders the heat conduction in the horizontal direction; 2) the composite thermal insulation layer of NPT and nanoscale water separates the steam generation layer from the water, reducing the vertical heat conduction. This structure increases the difficulty of transferring heat from the water near the hot spot to the entire water. We measured the water temperature (just under the samples) and steam temperature under same working conditions (Figure 4c). Under one sun, both the water and steam temperature of reversed structures (i-Au/NPT-ue, pe, and ce) are lower than that of the Au/NPT. This indicates that the samples can effectively prevent heat transfer to water below, and reduce wasting energy for high-temperature steam generation (A detailed calculation of steady-state energy balance can be found in Supporting Information). At same time, although completely etched device has advantages over partially etched in spectral input energy, thermal management has a greater impact on steam generation performance, so there is only 1% difference on efficiency of them. We further compare our result with previous NPT-based plasmonic evaporators, which shows an ≈20% increment on efficiency (Figure 4d). Our i-Au/NPT evaporator with a thickness of only tens of microns has reached the same efficiency level of those carbon-based evaporators with thickness of several centimeters. Meanwhile, by reducing the

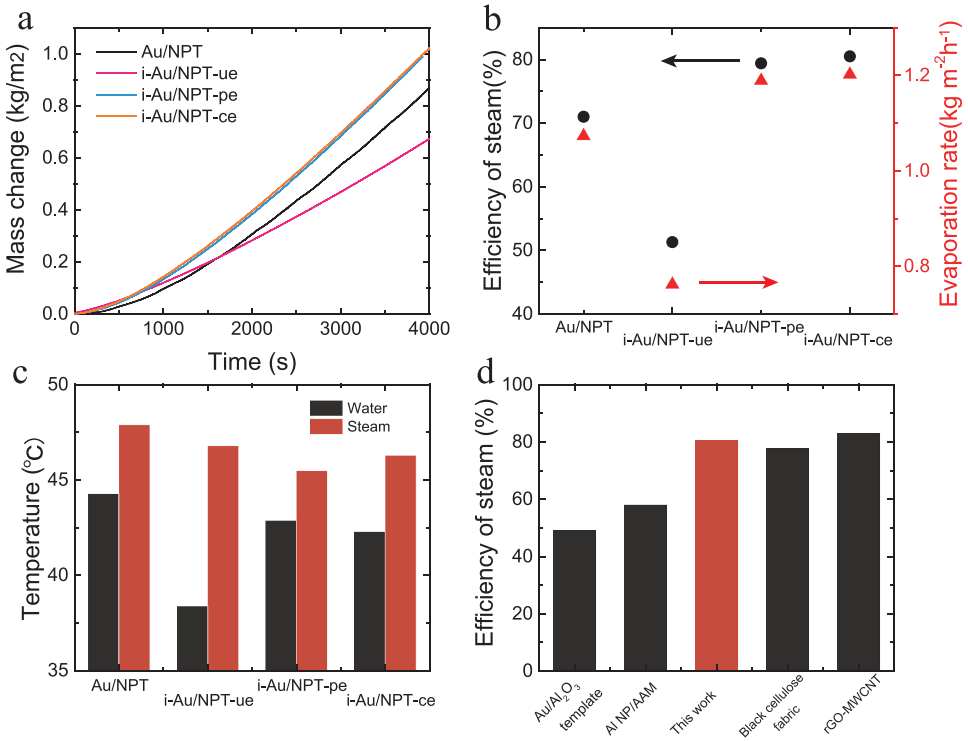

Figure 4. Solar steam characterization of Au-NPT-based evaporators. a) Mass change as a function of time. b) Energy transfer efficiency and evaporation rate. Au/NPT: 71%, 1.073 kg m^{-2} h^{-1}. i-Au/NPT-ue: 51.3%, 0.762 kg m^{-2} h^{-1}. i-Au/NPT-pe: 79.4%, 1.189 kg m^{-2} h^{-1}. i-Au/NPT-ce: 80.5%, 1.202 kg m^{-2} h^{-1}. c) Temperature of steam and water just under the evaporators. d) Comparison of different evaporators' efficiency under one sun. The data are extracted from ref. [24] (Au/Al_2O_3 template), ref. [13] (Al NP/AAM), ref. [21] (Black cellulose fabric), and ref. [29] (rGO-MWCNT).

thickness of NPT, the material can be flexible and the radiation loss caused by alumina can be reduced. These properties make our plasmonic evaporator have good potential in portable solar thermal conversion devices or other composite systems with finite space.

3. Conclusion

In conclusion, we demonstrate an ultrathin self-floating i-Au/NPT evaporator with enhanced spectral and thermal management for efficient solar steam generation. Through self-assembled Au nanoparticles' deposition and IBE techniques, an all-dielectric insulated 3D plasmonic nanoparticles structure is prepared with efficient and broadband solar absorption, reduced thermal loss, and enhanced mass transport. A solar–thermal conversion efficiency of ≈80% is achieved under one sun, with an evaporator thickness of only tens of microns. This work provides a new way for the regulation of optical and thermal properties of solar–thermal conversion materials, and inspires further development of solar steam generations.

4. Experimental Section

Fabrication Process for i-Au/NPT Structure: The nanoporous alumina template was fabricated by a two-step anodization method and then sputtered with gold nanoparticles by a PVD system (Gatan, model 682) with an effective thickness of 85 nm. The NPT (with thickness of ≈60 µm) possessed random sized nanopores with diameter mainly distributed at 330–400 nm so as to enable shallow Au film on top of the substrate and deep deposited Au nanoparticles inside the nanochannels (1.5–2 µm deep). The samples were then transferred into the IBE system (Beijing Chuangshiweina, IBE 150) to remove the surface Au film with an etching time of 2–6 min by an ion current of 75 mA to gradually approach the critical point where surface Au film was completely removed while the vertical Au NPs were well maintained.

Optical Measurements of the Au-NPT-Based Evaporators: The hemispherical optical transmittance (T) and reflectance (R) spectra of the Au-NPT-based evaporators were measured in the range of 200–2500 nm with a Shimadzu UV3600 spectrophotometer attached to an integrating sphere (ISR-3100). The absorptance (A) was then calculated by $A = 1 - R - T$. A Bruker Vertex 70 FTIR spectroscope was used for mid-infrared regime.

Solar Steam Measurements: The solar desalination experiments were performed under a solar simulator (Newport 94043A). In the experiment, the water was contained by a chamber (Dewar flask, 28-mm inner diameter, 38-mm outer diameter, and 96-mm height; Shanghai Glass Instrument Co.) and the Au-NPT-based evaporator floated on the surface of the water. The optical power on the sample surface was measured by a thermocouple power meter (Coherent 1097901). The mass change was measured by a high accuracy balance (FA 2004, 0.1 mg in accuracy) and then real-time communicated to a desktop computer for the evaluation of the evaporation rate. The temperature of the steam and water were measured by two thermocouples.

Supporting Information

Supporting Information is available from the Wiley Online Library or from the author.

Acknowledgements

Y.W. and H.M. contributed equally to this work. The authors acknowledge the micro-fabrication center of National Laboratory of Solid State Microstructures (NLSSM) for technique supports. This work was supported by the National Key Research and Development Program of China (2021YFA1400700 and 2022YFA1404300) and the National Natural Science Foundation of China (12022403, 61735008, and 11874211).

Conflict of Interest

The authors declare no conflict of interest.

Data Availability Statement

The data that support the findings of this study are available from the corresponding author upon reasonable request.

Keywords

plasmonic nanoparticles, solar evaporation, spectral regulation, thermal insulation

Received: August 16, 2022
Revised: December 21, 2022
Published online:

[1] W. Li, J. Valentine, *Nano Lett.* **2014**, *14*, 3510.
[2] S. Linic, U. Aslam, C. Boerigter, M. Morabito, *Nat. Mater.* **2015**, *14*, 567.
[3] N. Liu, M. Mesch, T. Weiss, M. Hentschel, H. Giessen, *Nano Lett.* **2010**, *10*, 2342.
[4] S. A. Maier, *Plasmonics: Fundamentals and Applications*, Springer, New York **2007**.
[5] A. Naldoni, V. M. Shalaev, M. L. Brongersma, *Science* **2017**, *356*, 908.
[6] O. Neumann, A. S. Urban, J. Day, S. Lal, P. Nordlander, N. J. Halas, *ACS Nano* **2013**, *7*, 42.
[7] H. Ghasemi, G. Ni, A. M. Marconnet, J. Loomis, S. Yerci, N. Miljkovic, G. Chen, *Nat. Commun.* **2014**, *5*, 4449.
[8] G. Ni, G. Li, S. Boriskina, H. Li, W. Yang, T. Zhang, G. Chen, *Nat. Energy* **2016**, *1*, 16126.
[9] H. Liang, Q. Liao, N. Chen, Y. Liang, G. Lv, P. Zhang, B. Lu, L. Qu, *Angew. Chem., Int. Ed. Engl.* **2019**, *58*, 19041.
[10] Y. Li, T. Gao, Z. Yang, C. Chen, W. Luo, J. Song, E. Hitz, C. Jia, Y. Zhou, B. Liu, B. Yang, L. Hu, *Adv. Mater.* **2017**, *29*, 1700981.
[11] J. Li, M. Du, G. Lv, L. Zhou, X. Li, L. Bertoluzzi, C. Liu, S. Zhu, J. Zhu, *Adv. Mater.* **2018**, *30*, 1805159.
[12] W. Li, Z. Li, K. Bertelsmann, D. E. Fan, *Adv. Mater.* **2019**, *31*, 1900720.
[13] L. Zhou, Y. Tan, J. Wang, W. Xu, Y. Yuan, W. Cai, S. Zhu, J. Zhu, *Nat. Photonics* **2016**, *10*, 393.
[14] N. Xu, J. Li, Y. Wang, C. Fang, X. Li, Y. Wang, L. Zhou, B. Zhu, Z. Wu, S. Zhu, J. Zhu, *Sci. Adv.* **2019**, *5*, eaaw7013.
[15] T. A. Cooper, S. H. Zandavi, G. W. Ni, Y. Tsurimaki, Y. Huang, S. V. Boriskina, G. Chen, *Nat. Energy* **2018**, *9*, 5086.
[16] Y. Xia, Q. Hou, H. Jubaer, Y. Li, Y. Kang, S. Yuan, H. Liu, M. W. Woo, L. Zhang, L. Gao, H. Wang, X. Zhang, *Environ. Sci.* **2019**, *12*, 1840.
[17] L. Wu, Z. Dong, Z. Cai, T. Ganapathy, N. X. Fang, C. Li, C. Yu, Y. Zhang, Y. Song, *Nat. Commun.* **2020**, *11*, 521.
[18] X. Zhou, F. Zhao, Y. Guo, Y. Zhang, G. Yu, *Energy Environ. Sci.* **2018**, *11*, 1985.
[19] A. Alabastri, P. D. Dongare, O. Neumann, J. Metz, I. Adebiyi, P. Nordlander, N. J. Halas, *Energy Environ. Sci.* **2020**, *13*, 968.
[20] X. Liu, Y. Xuan, *Nanoscale* **2017**, *9*, 14854.
[21] K. Bae, G. Kang, S. K. Cho, W. Park, K. Kim, W. J. Padilla, *Nat. Commun.* **2015**, *6*, 10103.
[22] Y. Liu, S. Yu, R. Feng, A. Bernard, Y. Liu, Y. Zhang, H. Duan, W. Shang, P. Tao, C. Song, T. Deng, *Adv. Mater.* **2015**, *27*, 2768.
[23] M. Zhu, Y. Li, F. Chen, X. Zhu, J. Dai, Y. Li, Z. Yang, X. Yan, J. Song, Y. Wang, E. Hitz, W. Luo, M. Lu, B. Yang, L. Hu, *Adv. Energy Mater.* **2018**, *8*, 1701028.
[24] L. Mascaretti, A. Schirato, R. Zbořil, Š. Kment, P. Schmuki, A. Alabastri, A. Naldoni, *Nano Energy* **2021**, *83*, 105828.
[25] L. Zhou, Y. Tan, D. Ji, B. Zhu, P. Zhang, J. Xu, Q. Gan, Z. Yu, *Sci. Adv.* **2016**, *2*, e1501227.
[26] L. Zhou, S. Zhuang, C. He, Y. Tan, Z. Wang, J. Zhu, *Nano Energy* **2017**, *32*, 195.
[27] C. Chen, L. Zhou, J. Yu, Y. Wang, S. Nie, S. Zhu, J. Zhu, *Nano Energy* **2018**, *51*, 451.
[28] J. Yu, L. Zhou, Y. Wang, Y. Tan, Z. Wang, S. Zhu, J. Zhu, *J. Opt.* **2018**, *20*, 034005.
[29] H. Gong, X. Liu, G. Liu, Z. Lin, X. Yu, L. Zhou, *Nanophotonics* **2020**, *9*, 1539.
[30] X. Li, W. Xu, M. Tang, L. Zhou, B. Zhu, S. Zhu, J. Zhu, *Proc. Natl. Acad. Sci. USA* **2016**, *113*, 13953.
[31] X. Hu, W. Xu, L. Zhou, Y. Tan, Y. Wang, S. Zhu, J. Zhu, *Adv. Mater.* **2017**, *29*, 1604031.
[32] C. Finnerty, L. Zhang, D. L. Sedlak, K. L. Nelson, B. Mi, *Environ. Sci. Technol.* **2017**, *51*, 11701.
[33] M. Zhu, Y. Li, G. Chen, F. Jiang, Z. Yang, X. Luo, Y. Wang, S. D. Lacey, J. Dai, C. Wang, C. Jia, J. Wan, Y. Yao, A. Gong, B. Yang, Z. Yu, S. Das, L. Hu, *Adv. Mater.* **2017**, *29*, 1704107.
[34] L. Zhou, X. Li, G. Ni, S. Zhu, J. Zhu, *Natl. Sci. Rev.* **2019**, *6*, 562.